

Control of Boundary Layer Streaks Induced by Freestream Turbulence Using Plasma Actuators

Kevin A. Gouder

Department of Aeronautics
Imperial College London
SW7 2AZ, London, U.K.
kevin.gouder04@imperial.ac.uk

Ahmed M. Naguib

Department of Mechanical Engineering
Michigan State University
MI 48824, USA
naguib@egr.msu.edu

Philippe L. Lavoie

Institute for Aerospace Studies
University of Toronto
Toronto, ON M3H 5T6, Canada
lavoie@utias.utoronto.ca

Jonathan F. Morrison

Department of Aeronautics
Imperial College London
SW7 2AZ, London, U.K.
j.morrison@imperial.ac.uk

ABSTRACT

Previously, a systematic series of investigations, such as those of Hanson *et al.* (2010), Hanson *et al.* (2014) and Bade *et al.* (2016) were carried out aimed at assessing the capability of plasma-actuator-based Feedforward-Feedback control system to weaken streaks that were artificially induced into a Blasius boundary layer using dynamic roughness elements. In contrast, the current work builds on these previous works and drives towards the delay of bypass boundary layer transition, where in the presence of a freestream flow with turbulence intensity exceeding approximately 1%, streaks form naturally and stochastically in the underlying boundary layer. For the freestream velocity of the current experiment, turbulent spot formations were first observed at a streamwise location $x \approx 350$ mm from the leading edge. Upstream of this location, the naturally-occurring high and low-speed streaks exhibit linear transient growth. Two wall-shear-stress sensors – one feedforward (FF) and one feedback (FB) – and two plasma actuators capable of producing positive and negative wall-normal forcing to oppose high and low-speed streaks respectively were placed in the linear growth region. The output from the FF sensor was used in conjunction with single-point Linear Stochastic Estimation (LSE) and actuator-flow identified response models in order to generate a counter-disturbance, which, at the (downstream) FB sensor location, was equal in magnitude but opposite in sign to the natural streak estimate. The output of the FB sensor was fed to a PI controller to correct for any remaining, uncancelled disturbance resulting from, for example, inaccuracies in the LSE model of streak growth. Results, such as notable changes in the mean and rms wall normal velocity profiles and energy spectra, for FF only, and FF + FB control, provide an evaluation of the viability of the control approach to weaken boundary layer streaks and delay transition.

INTRODUCTION

The formation and the growth of streamwise elongated velocity disturbances, commonly referred to as streaks, or Klebanoff distortions, mark the beginning of bypass boundary layer transition, Zaki (2013). Sensing and cancellation of streaks early within their growth extent could enable the suppression or delay of bypass transition and eventual turbulence. Jacobson & Reynolds (1998) provided an early experimental demonstration of weakening of steady streaks through the generation of a pair of counter-rotating vortices opposite in sign to an artificial pair generated further upstream by

a circular cylinder, and also, weakening of unsteady streaks introduced by suction. Lundell (2007) demonstrated successful bypass transition delay using wall-shear sensing, manually-tuned Feedforward control and actuation through suction and blowing. Control of the transient growth of streaks introduced by a spanwise array of static cylindrical roughness elements in a Blasius boundary layer was demonstrated by Hanson *et al.* (2010) using plasma actuators. In a follow-up experiment, Hanson *et al.* (2014) demonstrated proportional integral (PI) feedback control where sensing and control of steady but slowly varying streaks was implemented. Bade *et al.* (2016) reported further developments: unsteady streaks generated in the boundary layer by a single dynamically activated roughness element were sensed, and a model-based controller for the boundary layer dynamics determined the output for their suppression.

The current work builds on this previous work and drives towards the delay of bypass boundary layer transition. The setup uses wall-shear stress sensors, one upstream and one downstream of a plasma actuator. Model-based controllers are derived from empirical data and are used to tune Feedforward and Feedback controllers.

EXPERIMENTAL SETUP

The experiments were carried out in a closed-return wind tunnel with a test section measuring 457 mm square. A sharp leading edge Blasius-boundary-layer test-plate was mounted horizontally across the width of the wind tunnel and a bi-planar grid introduced freestream turbulence of approximately 2.5% intensity at the plate leading edge. At the freestream velocity of the current experiments, 6 ms^{-1} , turbulence spot formation started at $x \approx 350$ mm from the leading edge. Upstream of $x \approx 350$ mm the streaks exhibit linear transient growth and a combined FF-FB system is employed within this linear region with an aim of weakening the streaks. The FF system uses input from a wall-mounted hot-wire, S_U , installed upstream of a plasma actuator. This sensor detects streaks in their early stages of growth and the sensor output is used in conjunction with Linear Stochastic Estimation (LSE) to estimate the streaks' streamwise shear disturbance τ_D' at a downstream x location where a second wall-mounted hot-wire, S_D , is installed. This estimate is used to modulate the plasma actuator voltage in order to produce a counter-disturbance which, at S_D , is equal in magnitude and opposite in sign to the estimate. If S_D still registers a residual disturbance, i.e. τ_D' is not completely driven to zero, for example, due to inaccuracies in the streak dynamics model, including the LSE

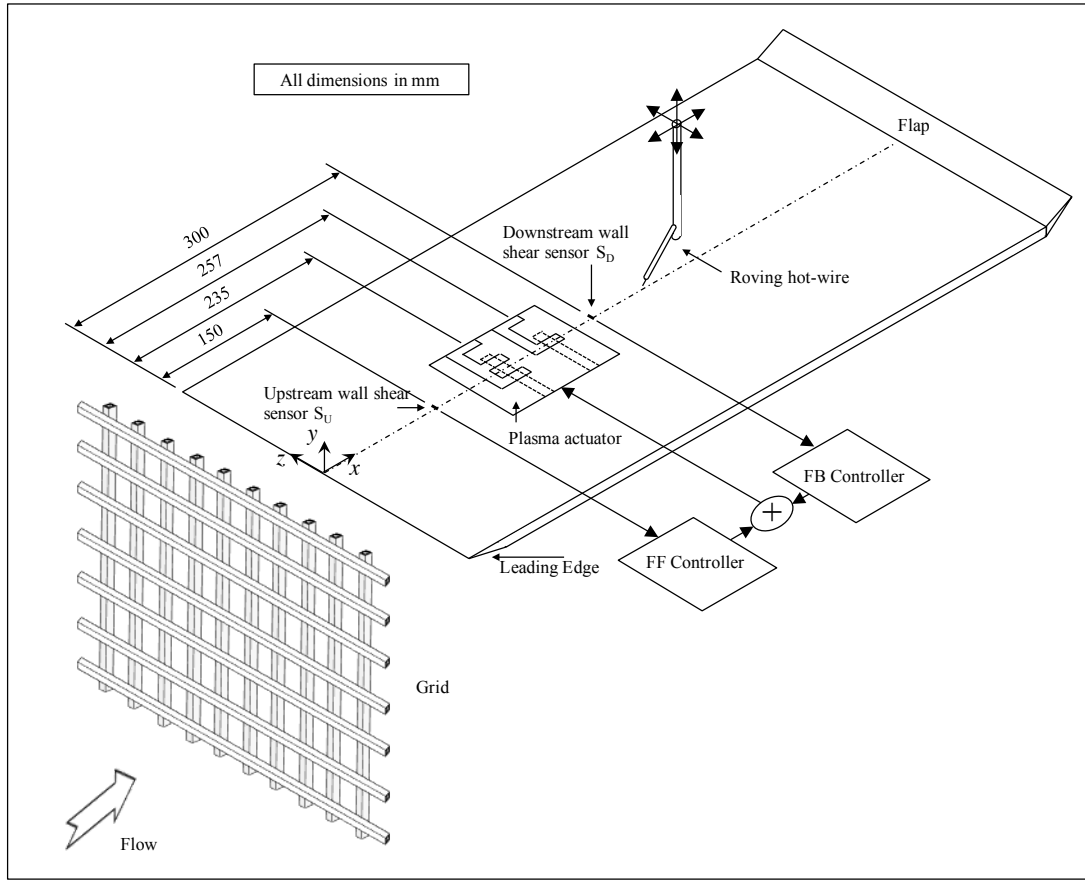


Figure 1. Schematic of the experimental configuration.

estimation, its output (the error) is fed back to a feedback PI controller to optimise the plasma actuator voltage for better cancellation. Figure 1 shows a schematic of the experimental arrangement. The three hot-wires (two wall-mounted ones and one roving) are driven by a Dantec Streamline Pro CTA and signals from these sensors are acquired by a National Instruments PXI Real-Time system. The plasma actuator consists of two sub-actuators: with reference to Figures 1 and 2, the F-shaped actuator (designated α , upstream) is used for high-speed-streak control; the Γ -shaped actuator (designated β , downstream) is used for low-speed-streak control. Each sub-actuator is driven by a TREK 609E6 high voltage amplifier receiving an input sine wave of 3 kHz. The strength of the actuation could be varied by amplitude modulation of the sine wave. The modulation signals are provided by the analogue-output channels of the Feedforward and Feedback controllers on the PXI real-time system in response to the wall-shear sensor inputs.

CONTROL MODEL

A block diagram with the details of the FF control system is shown in Figure 4. From the left-hand side, the wall-normal velocity fluctuations v'_{FS} produced by the freestream turbulence generated by the grid lead to the formation of unsteady low-speed streaks in the boundary layer through the Orr-Sommerfeld / Squire dynamics. This is manifested as a fluctuating wall-shear stress τ'_U as measured by the upstream sensor S_U . Through the boundary layer linear dynamics, $P_{\tau_U \tau_D}$ the streaks grow and produce the fluctuating shear stress τ'_D at the downstream sensor S_D . In order to nullify the disturbance, the τ'_U signal is fed to the upper or lower branches of the controller in Figure 4, depending on the polarity of τ'_U (subscripts α and β correspond respectively to the high-speed and low-speed streak control). The signal is low-pass filtered at 1 kHz, an

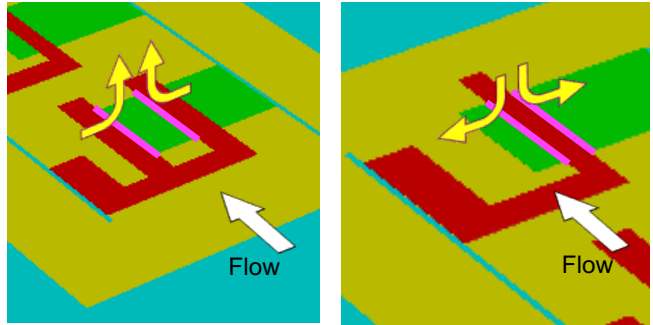


Figure 2. A schematic of the two plasma actuators consisting of high voltage electrodes (in red) and low voltage electrodes (in green) separated by Kapton tape. The plasma is indicated by the magenta stripes. The flow each actuator induces is shown: the F-shaped actuator blows away from the wall and generates a low-speed streak and is hence used for high-speed streak control. The Γ -shaped actuator sucks towards the wall and generates a high-speed streak and is hence used for low-speed streak control.

order of magnitude above the streaks disturbance bandwidth, and is then fed to the FF controller $C_{FF,\alpha}$ (or $C_{FF,\beta}$). C_{FF} consists of two transfer functions. The first of these functions is ideally set to the physical $P_{\tau_U \tau_D}$ so that in response to an input τ'_U , an output of magnitude τ'_D is produced. The boundary layer transition growth dynamics are however unknown and are therefore approximated by $\tilde{P}_{\tau_U \tau_D}$. In the present work, $\tilde{P}_{\tau_U \tau_D}$ is based on LSE and determined prior to the control experiment through the simultaneous measure-

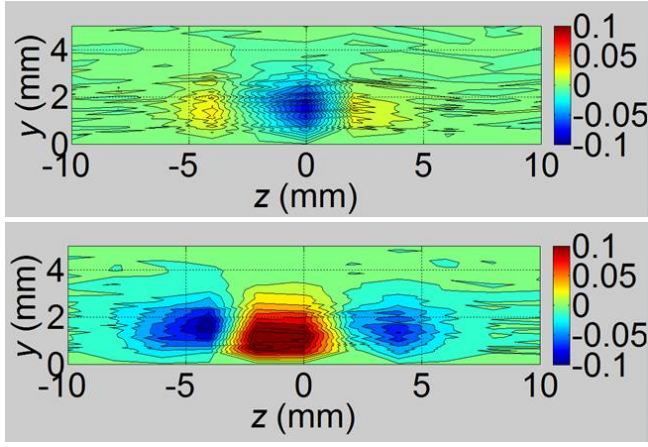


Figure 3. The disturbances generated by the two actuators: (top) the low speed streak generated by the F-shaped actuator; (bottom) the high speed streak generated by the Γ -shaped actuator.

ments of τ'_U and τ'_D . The second transfer function in the controller uses the estimate of τ'_D as input to determine the required actuator's peak-to-peak voltage (V_{pp}) to generate the estimated disturbance. This requires knowledge of the inverse of the transfer function $P_{V\tau_D}$ relating the voltage input to the actuator to the generated τ'_D disturbance. $P_{V\tau_D}$ is approximated prior to the control experiment through step-response tests where a step change in V_{pp} is imposed and the response τ_D is recorded. The output of $\tilde{P}_{V\tau_D}^{-1}$ is the required peak-to-peak voltage to produce the desired τ'_D counter disturbance to the streak. This voltage is converted into a modulating voltage v_m to the function generator that generates the amplitude-modulated sinusoidal signal to the high-voltage amplifiers that drive the actuators. The relation between V_{pp} and v_m is determined prior to the control experiment.

To approximate the transfer function $\tilde{P}_{\tau_U\tau_D}$, the cross-correlation coefficient $R_{\tau_U\tau_D}$ between τ'_U and τ'_D is computed. Figure 5 shows there is a substantial linear correlation, of about 0.6, between the upstream and downstream shear signals with a delay of about 38 ms corresponding to the convection of the disturbance from S_U to S_D . Delaying the τ'_U signal by 38 ms, single-point LSE is used to predict τ'_D : the LSE coefficient is used in conjunction with the time delay to approximate $\tilde{P}_{\tau_U\tau_D}$ as:

$$\tilde{P}_{\tau_U\tau_D}(s) = K_\tau e^{-t_{d\tau}s} = \frac{r_{\tau_U\tau_D,max}}{\tau_{U,rms}^2} e^{-t_{d\tau}s} \quad (1)$$

where $r_{\tau_U\tau_D,max}$ is the peak correlation and $t_{d\tau}$ is a time delay equal to the peak correlation time delay. Figure 6 shows a sample comparison between the actual shear signal τ'_D and the one estimated from τ'_U using LSE; agreement varies from very good to none at all.

To approximate the transfer function $\tilde{P}_{V\tau_D}^{-1}$ actuator step response tests were conducted prior to the control experiment. Figure 7 shows sample results for the high-speed streak control (α) actuator. The figure shows the temporal evolution of the wall shear τ_D for different step voltage inputs as measured by S_D for a voltage which comes on at 0 seconds and off at 0.5 seconds. The response is modelled as a time-delayed first-order system response. The parameters of the model were found to be reasonably independent of step input size and this supported the hypothesis of the boundary layer's linear response, at least within the actuator voltage range. The model

transfer function (here for the α actuator) is:

$$\tilde{P}_{V\tau_D,\alpha}(s) = \frac{K_{V,\alpha}}{t_{cV,\alpha}s + 1} e^{-t_{dV,\alpha}s} \quad (2)$$

where $K_{V,\alpha}$ is a static gain, $t_{dV,\alpha}$ is a time delay corresponding to the convection of the disturbance from the sub-actuator to S_D (different for α and β), and $t_{cV,\alpha}$ is a time constant.

The FF controller is obtained by combining equations 1 and 2. For the α actuator this takes the form:

$$C_{FF,\alpha}(s) = \tilde{P}_{\tau_U\tau_D}(s) \tilde{P}_{V\tau_D,\alpha}^{-1}(s) = \frac{K_\tau}{K_{V,\alpha}} (t_{cV,\alpha}s + 1) e^{-(t_{d\tau} - t_{dV,\alpha})s} \quad (3)$$

Following either the α or β route in Figure 4 it is evident that the effectiveness of the FF control hinges on the accuracy of the models of $\tilde{P}_{\tau_U\tau_D}$ and $P_{V\tau_D,\alpha}$ (or $P_{V\tau_D,\beta}$).

If following the FF control, S_D still registers a remnant disturbance, i.e. $\tau'_{D,c}$ (the subscript c denoting 'controlled') is not completely driven to zero, for example, due to inaccuracies in the streak dynamics model, its filtered output (the error) is fed to a PI controller, discriminating on the polarity of the residual $\tau'_{D,c}$, to effectively adjust the plasma actuator voltage. This combined FF+FB controller implementation is shown in Figure 8. Labview built-in anti-windup prevents the integral part of the Feedback controller from accumulating error when the voltage input demand to the actuator is outside the set control voltage range, i.e. in cases where the disturbance is too large to be controlled within the operating voltage limits of the plasma actuator.

The parameters required for correct operation of the PI controller were a gain K_{fb} and an integral time $t_{I,fb}$ which were set according to the tuning rules and recommendations in Skogestad (2003) and the plant model for the plasma actuator. The feedback controller transfer function is given by:

$$\frac{F_{fb}(s)}{\tau'_D(s)} = C_{\tau'_U,fb} = K_{fb} \frac{t_{I,fb}s + 1}{t_{I,fb}s} \quad (4)$$

where K_{fb} is the controller gain, $F_{fb}(s)$ is the feedback output and $\tau'_D(s)$ is the shear stress disturbance at S_D in the Laplace domain. The controller gain is given by (Skogestad (2003)):

$$K_{fb} = \frac{0.5 t_{cV}}{k_{fb} t_{dV}} \quad (5)$$

$k_{fb} = 1$ for all streamwise locations of the feedback sensor S_D , as reported in Bade *et al.* (2016).

The integral time, (Skogestad (2003)) is given by:

$$t_{I,fb} = \min\{t_{cV}, 8t_{dV}\} \quad (6)$$

which effectively means that $t_{I,fb} = t_{cV}$, since in all cases the time constant t_{cV} was smaller than the time delay t_{dV} .

The feedback control is expected to work on the principle that if the remnant of a streak has reached the sensor S_D but it is also still partly over the plasma actuator, then the actuator voltage can be adjusted to further drive $\tau'_{D,c}$ to zero. This implies that i) there is a minimum streak length that can be controlled and, ii) there is a delay associated with the convection time of the disturbance from the actuator to S_D .

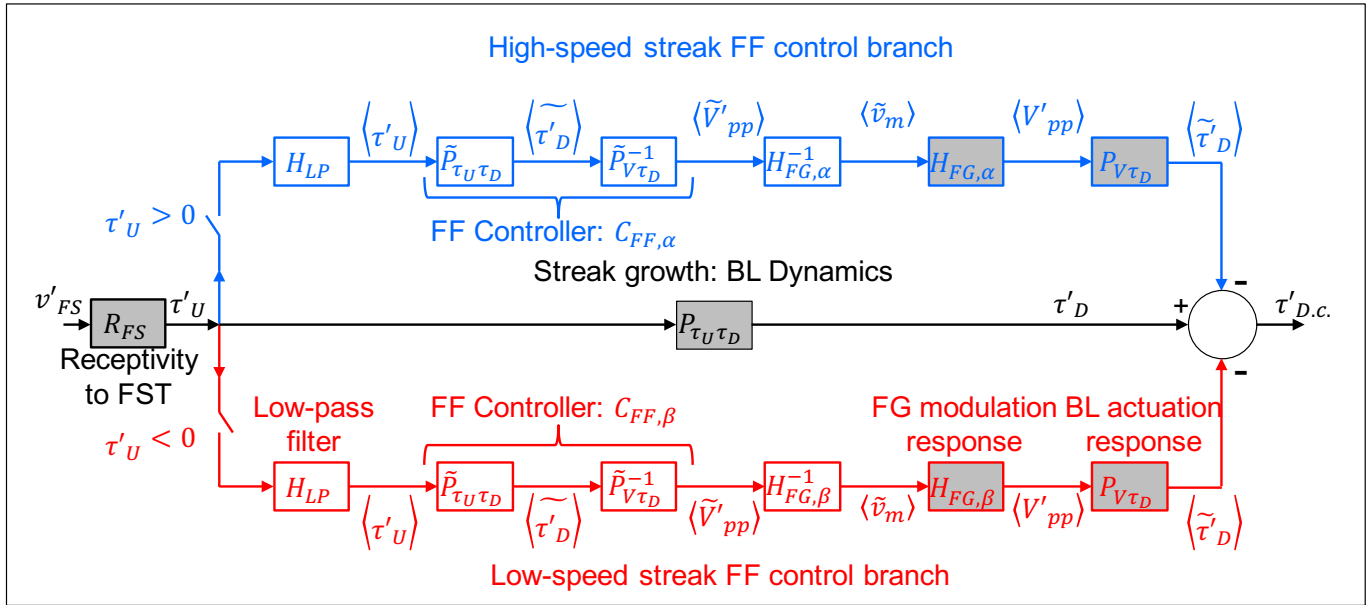


Figure 4. Block diagram of the implemented FF control system. Angle bracketed symbols represent low-pass filtered quantities. Tilde accents denote an estimate. Grey-shaded blocks represent physical systems. The remaining blocks represent dynamics simulated using LabView code running on a National Instruments real-time system.

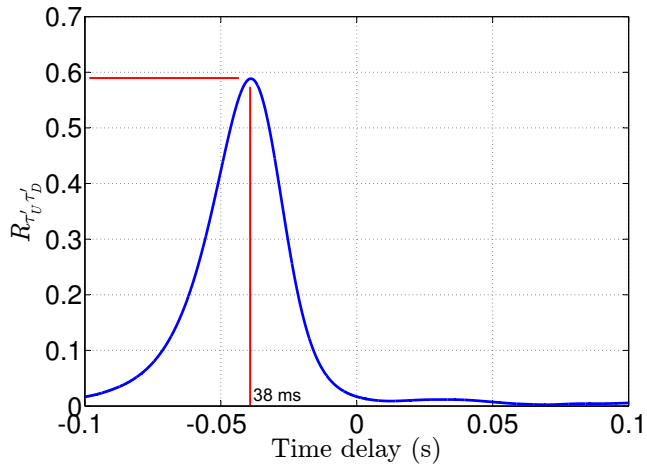


Figure 5. Cross-correlation coefficient between the upstream and downstream shear signals.

RESULTS

A number of experiments were conducted; ones where only the FF control system was operational, others where combined FF+FB controllers were used and others where only the FB controller was used. In each case, voltage measurements made by S_D were used as a metric to assess streaks suppression capability. The power spectral density (PSD) of the signal recorded at S_D for the different control scenarios are shown in Figure 9. Successful streak weakening was achieved when the FF controller was used; the r.m.s. of the streamwise fluctuations at S_D was lowered by 19% (34.7% reduction in energy). This corresponds to the suppressed PSD traces shown in Figure 9 labelled “FF Control Gain = 1” when compared to the “No Control” trace. Gain = 1 indicates that the gain of the controller driving the α (or β) actuator was equal to the value indicated by the term $\frac{K_\tau}{K_{V,\alpha}}$ (or $\frac{K_\tau}{K_{V,\beta}}$) in equation 3. The gain of the FF controller was raised to 1.5, i.e. $1.5 \times \frac{K_\tau}{K_{V,\alpha}}$ ($1.5 \times \frac{K_\tau}{K_{V,\beta}}$). A marginally

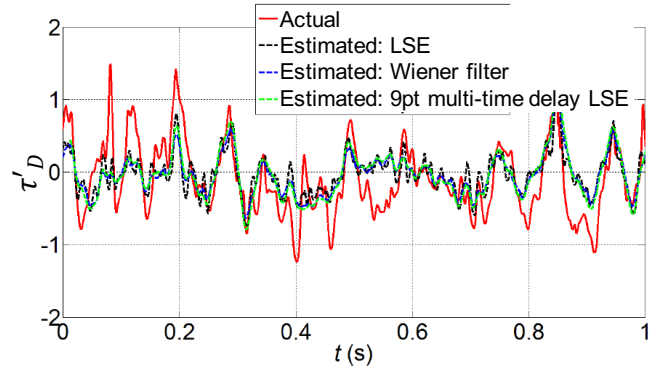


Figure 6. A sample comparison between the actual shear signal τ'_D and the one estimated from τ'_U using various methods including the current LSE. More advanced methods may yield a better estimate but may be too computationally expensive for a real-time control application. The long-time correlation coefficient between the two signals is approximately 50%.

better reduction in the r.m.s value at S_D , 20.5%, was registered, also seen in Figure 9 in the PSD trace labelled “FF Gain = 1.5”. While the “FF Gain = 1.5” trace is suppressed further than the “FF Gain = 1” trace for frequencies lower than about 11 Hz, the two traces cross each other and the “FF Gain = 1.5” remains slightly higher thereafter.

The combined FF+FB controller was then introduced, initially with both the FF and FB gains (see equation 5) maintained at 1. Although the reduction in the r.m.s. of the signal at S_D diminished by only 13% despite the supposedly better control capability, the PSD of the signal in Figure 9, labelled “FF Gain = 1; FB Gain = 1”, reveals that the combined FF+FB control (both with Gain = 1) is far superior than the FF control on its own (even when a higher gain of 1.5 was utilised for the FF control) for frequencies up to about 9 Hz. However for higher frequencies, the combined FF+FB Gain

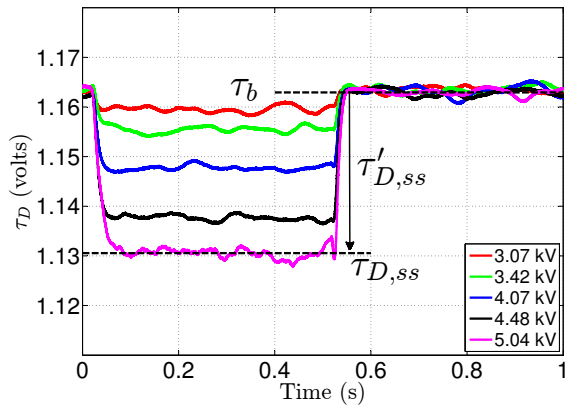


Figure 7. Sample results from the step response tests on the high-speed streak control actuator. τ_b denotes the Blasius (undisturbed) output of S_D and subscript ss indicates steady-state. Note that the voltage comes ON at time = 0 s and OFF at 0.5 s.

= 1 trace climbs above the FF only traces and indeed, eventually, above the “No Control” trace.

The FF gain was maintained at 1 but the FB gain was lowered to 0.6 (i.e. the FB controller gain was set to $K_{fb} = 0.3 \frac{t_{av}}{t_{av}}$). Now, the r.m.s. of the signal at S_D diminished by 19% equaling the Feedforward, Gain = 1 controller, and the PSD trace labelled “FF Gain = 1; FB Gain = 0.6” again reveals the combined controller’s far superior performance in comparison to the FF only controllers up to a frequency of about 8.5 Hz. A further combined FF+FB experiment was carried out where the FF control gain was raised to 1.5 while the FB gain was maintained at 0.6. The PSD trace for this case is labelled “FF Gain = 1.5; FB Gain = 0.6” revealing that the superior control at lower frequencies is maintained while the amplification of the higher frequencies is less pronounced.

The performance of the FB controller on its own was assessed in tests where the FF controller was switched off. The PSD traces labelled “FB Gain = 0.6” and “FB Gain = 1” reveal that that the FB controller on its own is superior to the FF controller, at least for low frequencies, but again, higher frequencies are amplified.

The 9 Hz point at which the combined FF+FB control is no longer better than the FF controller is believed to be the bandwidth limit of the current system, a limit appearing due to the finite distance between the actuator and S_D . The FB system will introduce an added control advantage for streaks of a streamwise length larger than this actuator-sensor distance; the FB adjustment will affect remnant streaks still lying above the actuator but already sensed by S_D . The actuator- S_D distance is interpreted as a bandwidth low-pass cutoff on the control system. The amplification of higher frequencies above the bandwidth limit is sometimes termed the “water-bed effect” or Bode’s integral formula which states that if disturbance attenuation is improved in one frequency range, it will be worse in another, Murray (2007). How the strong streak suppression at lower frequencies and the undesirable amplification of the higher frequencies contribute to intermittency, the formation of turbulent spots and

eventual turbulence further downstream is currently being analysed.

CONCLUSIONS

This paper reports the experimental implementation of a combined Feedforward-Feedback control scheme for weakening naturally-occurring streaks in a Blasius boundary layer while in their linear stages of growth, with the aim of delaying bypass transition to turbulence. The streaks were weakened by the plasma actuator that generated counter-disturbance streaks of estimated equal magnitude and opposite sense to those detected. The various control models were designed using empirical input-output data and LSE. Experimental results demonstrated the system effectiveness through a reduction of about 19% in r.m.s. streamwise velocity or 34.7% in energy at the downstream wall-shear sensor location in the FF only configuration. However, a comparison of the spectra for the FF only and FF+FB cases revealed that the latter controller was more than twice as effective as the FF controller on its own, at least in the lower frequency range within the (FF+FB)’s bandwidth. This reveals the dependence of the system bandwidth capability on the location of the downstream wall shear sensor (used for feedback), relative to the plasma actuator. Detailed changes in the mean and r.m.s. wall normal velocity profiles, energy spectra, probability density functions, intermittency and location of turbulent spot formation for FF only, FF+FB control, and FB only controllers, and the evolution of these changes with increasing streamwise coordinate x provide a detailed evaluation of the viability of this control approach. These metrics are currently being compiled and will be presented at the conference.

REFERENCES

- Bade, Kyle M., Hanson, Ronald E., Belson, Brandt A., Naguib, Ahmed M., Lavoie, Philippe & Rowley, Clarence W. 2016 Reactive control of isolated unsteady streaks in a laminar boundary layer. *Journal of Fluid Mechanics* **795**, 808–846.
- Hanson, Ronald E., Bade, Kyle M., Belson, Brandt A., Lavoie, Philippe, Naguib, Ahmed M. & Rowley, Clarence W. 2014 Feedback control of slowly-varying transient growth by an array of plasma actuators. *Physics of Fluids* **26** (2).
- Hanson, Ronald E., Lavoie, Philippe, Naguib, Ahmed M. & Morrison, Jonathan F. 2010 Transient growth instability cancellation by a plasma actuator array. *Experiments in Fluids* **49** (6), 1339–1348.
- Jacobson, Stuart A. & Reynolds, William C. 1998 Active control of streamwise vortices and streaks in boundary layers. *Journal of Fluid Mechanics* **360**, 179–211.
- Lundell, Fredrik 2007 Reactive control of transition induced by free-stream turbulence: an experimental demonstration. *Journal of Fluid Mechanics* **585**, 41–71.
- Murray, K.J. Åström & R.M. 2007 *Feedback Systems: An Introduction for Scientists and Engineers*. Princeton University Press.
- Skogestad, Sigurd 2003 Simple analytic rules for model reduction and {PID} controller tuning. *Journal of Process Control* **13** (4), 291 – 309.
- Zaki, Tamer A. 2013 From streaks to spots and on to turbulence: Exploring the dynamics of boundary layer transition. *Flow, Turbulence and Combustion* **91** (3), 451–473.

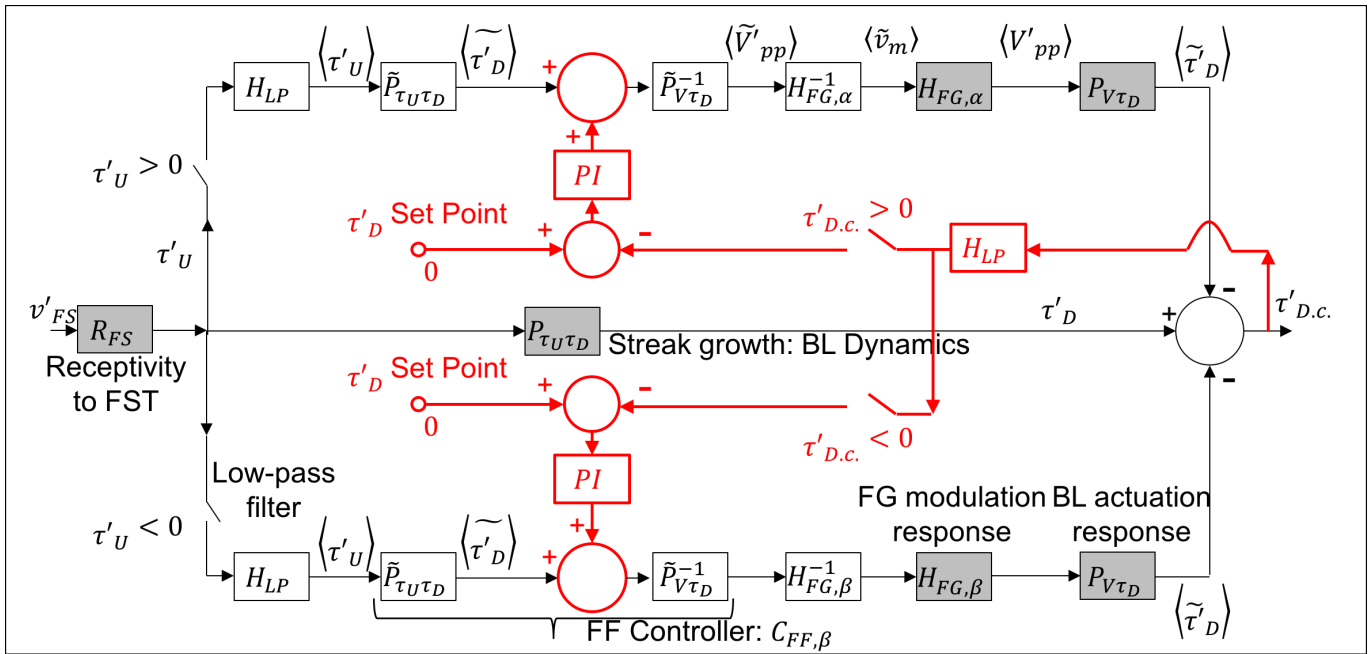


Figure 8. Block diagram of the implemented FF + FB control system. Meaning of symbols is the same as in Figure 4.

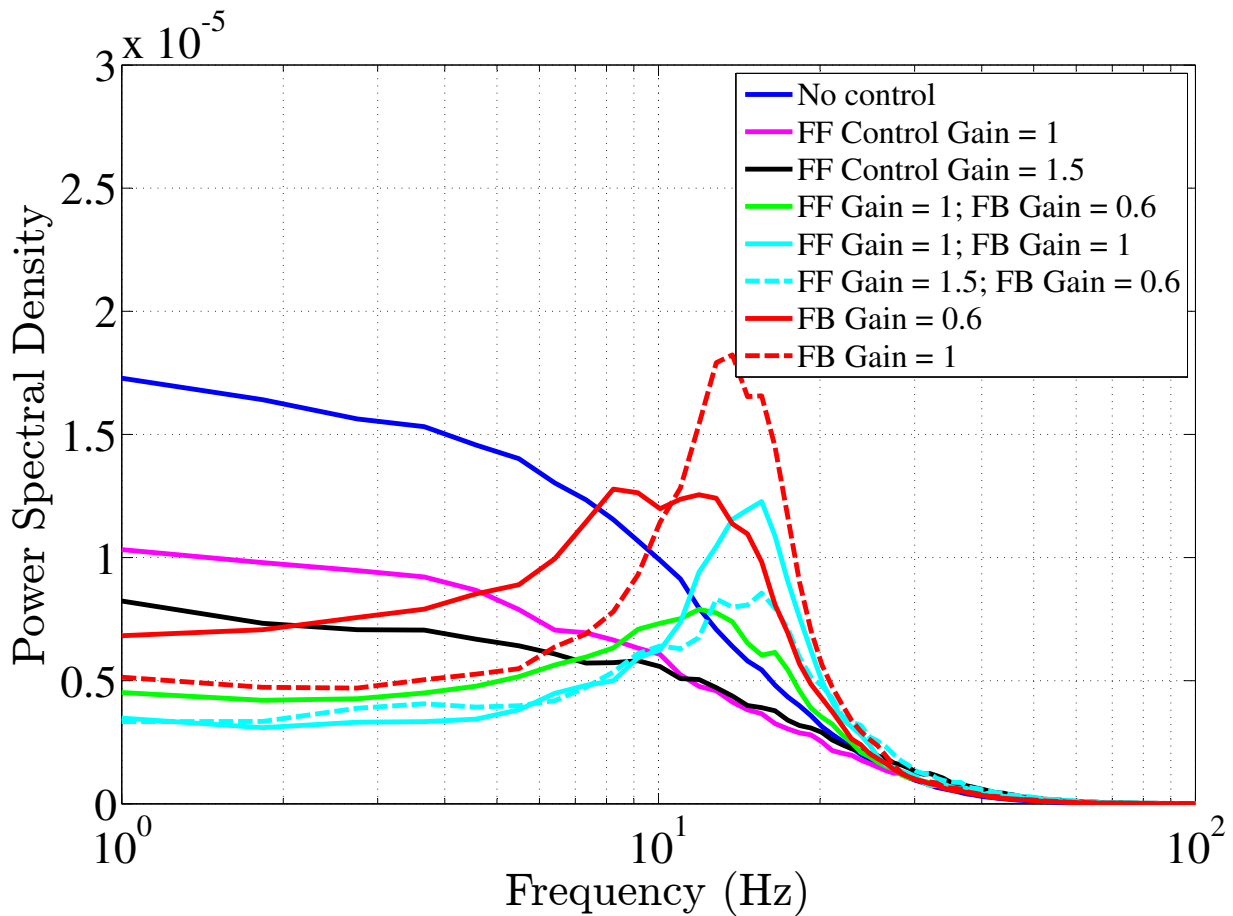


Figure 9. Spectra of the signal recorded by S_D for different control scenarios.